Instabilities of flows through deformable tubes and channels

O. E. Jensen

School of Mathematical Sciences, University of Nottingham, University Park, Nottingham NG7 2RD, UK Oliver.Jensen@nottingham.ac.uk

Flow driven through a segment of flexible tube, supported between rigid pipes and enclosed in a pressurized chamber, is susceptible to a variety of self-excited oscillations. This paper provides a brief review of recent modelling efforts aimed at understanding some of the underlying mechanisms of instability in this system. In particular, it is shown how a family of spatially one-, two- and three-dimensional models have been used to investigate a global instability arising at high frequencies, whereby axial sloshing motions driven by transverse wall oscillations are able to sustain themselves by extracting kinetic energy from the underlying mean flow.

1 Introduction

Fluids are distributed around the human body via networks of flexible tubes, and accordingly flow-structure interaction plays an important role in a number of biomedical transport phenomena. Flow limitation, for example, is well known to clinicians: collapse of veins above the heart (because of reduced hydrostatic pressure in an upright individual) limits return of blood to the heart — a particular concern for giraffes [1] — and flow-induced collapse of asthmatic airways inhibits expiration from the lung. Collapse of an elastic tube such as a vein or airway is likely to involve a buckling instability. Under positive transmural (interior minus exterior) pressure, the tube is circular in cross section and strongly resists area change; however under negative transmural pressure, the tube buckles (for example to an elliptical cross section) and becomes much more compliant. In the buckled state, there is potential for significant interaction between internal fluid flows and the elastic wall, and instabilities are commonplace. In the body, these are manifested for example as Korotkoff sounds (oscillations of the collapsed brachial artery underneath a blood-pressure cuff inflated around the upper arm) and wheezing during forced expiration [2, 3].

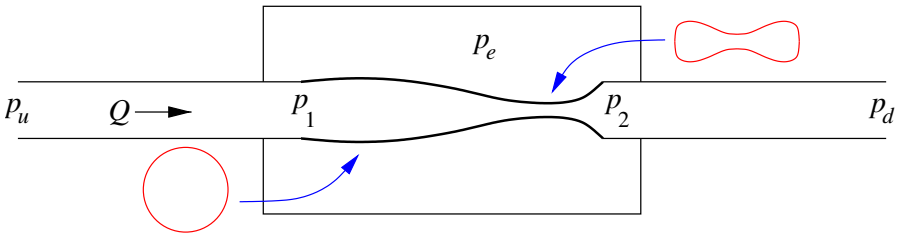

Fig. 1. The Starling Resistor. A flux Q is driven from left to right by a pressure drop between inlet and outlet (at pressures p_u and p_d respectively). The collapsible segment of tube is subject to external pressure p_e and may buckle to a non-axisymmetric cross-section when collapsed, as indicated.

The Starling Resistor [4] is a bench-top device that has been used to illustrate these phenomena to medical students for many years, and which has inspired and challenged researchers in biofluid-mechanics since the 1960s. A segment of elastic tube is mounted between two rigid tubes (Fig. 1). Flow is driven through the system either under a fixed pressure drop $p_u - p_d$, or with fixed volume flux Q. A chamber enclosing the flexible segment is raised to pressure p_e, causing collapse of the tube. When carrying a flow, the viscous pressure drop along the flexible segment causes the tube to collapse first towards its downstream end as p_e is increased. The pressures at the upstream and downstream ends of the flexible segment (p_1, p_2) are typically recorded experimentally. The steady flow properties of the system are strongly nonlinear: sucking on the downstream end of the tube (increasing $p_1 - p_2$ for fixed $p_1 - p_e$) leads to flow limitation, i.e. a maximum possible flux Q; blowing on the upstream end of the tube (increasing Q while holding $p_2 - p_e$ fixed) leads to saturation of the pressure drop $p_1 - p_2$. Self-excited oscillations arise during these manoeuvres in many regions of parameter space, even at modest Reynolds numbers (e.g. 300-500) if the tube wall is sufficiently thin. The oscillations fall into distinct frequency bands, exhibit a variety of characteristic nonlinear waveforms and depend strongly on the properties of the rigid parts of system (such as the lengths of the upstream and downstream rigid segments). The dynamics of the system have been carefully characterised experimentally by Bertram and co-workers [5, 6].

The present paper provides a review of some recent theoretical developments aimed at understanding the possible mechanisms of self-excited oscillation. The discussion is confined to a specific parameter regime in which the internal flow is below Reynolds numbers at which there is transition to turbulence, and for which fluid inertia dominates wall inertia (high-frequency flutter modes associated with wall inertia are not considered). The primary mechanical ingredients in all models discussed below are wall elasticity, fluid inertia (throughout the entire system) and viscous dissipation. The problem illustrates the value — and limitations — of relatively elementary models

in informing more sophisticated approaches. Accordingly, the discussion progresses from spatially one-dimensional (1D) models, which are useful in exploring the relationship between local and global instabilities and in providing an overview of parameter space (§3), through 2D models, in which oscillation thresholds can be predicted using high Reynolds-number asymptotics (§4), through to recent developments in 3D (§5). Comprehensive reviews of earlier studies and a more general account of relevant biomedical applications are provided in [2, 3, 7].

2 Models of flow in the Starling Resistor

It is helpful to put the discussion to follow into context by taking a brief overview of the different modelling approaches that have been used to address flow in the Starling Resistor.

Initial zero-dimensional (lumped-parameter) models described the system using a small set of time-dependent variables, incorporating approximate statements of mass and momentum conservation and a simple 'tube law' to model wall elasticity. By incorporating the basic mechanical ingredients mentioned above, Bertram & Pedley [8] for example were able to reproduce self-excited oscillations, and later models were shown to exhibit nontrivial dynamics [9]. However the inability to capture wave propagation is a fundamental limitation of this approach, and motivated the development of 1D models. These involve two coupled PDEs in the tube area $\alpha(x,t)$, cross-sectionally averaged axial velocity $u(x,t)$ and internal pressure $p(x,t)$ [10, 11]. However in this framework there is (inevitably) an *ad hoc* representation of viscous dissipation (either distributed along the tube [12] or associated with a separated internal jet [11]) and of the tube elasticity, for which a modified tube law of the form $p - p_e = P(\alpha) - T\alpha_{xx}$ is commonly used, where T represents axial tension and P is a nonlinear function capturing the dependence of compliance on the degree of tube collapse. 1D models predict multiple steady tube configurations in the presence of axial flow [13] and distinct oscillatory modes (numbered $2, 3, 4, \ldots$ according to the number of area extrema) arising in overlapping regions of parameter space, appearing in distinct frequency bands [14].

Given the inherent complexity of the Starling Resistor, involving as it does non-axisymmetric tube buckling coupled to unsteady separating 3D internal flow, much attention has focussed on a simpler 2D problem, first addressed by Pedley [15]. This involves a finite-length channel, one wall of which contains a segement of flexible membrane (see Fig. 2 below). While the device has yet to be realised in any physical experiment, because of the difficulty of constructing genuinely 2D flow conditions, it has nevertheless been investigated fruitfully by both asymptotic and numerical modelling approaches. Guneratne & Pedley [16] explored steady flow at high Reynolds numbers, using interactive boundary-layer theory, which captures weak flow reversal beyond

constrictions. They demonstrated multiple static solutions in modes $1, 2$, etc., bifurcating from the uniform state via transcritical bifurcations or through saddle-node bifurcations when the symmetry of the base state was perturbed by non-zero external pressure. The model revealed regions of parameter space in which no steady state could exist. Unsteady flows in the 2D analogue of the Starling Resistor have been captured in a series of papers using finite-element methods by Luo, Pedley and co-workers [17, 18]. Here oscillatory modes 2, 3, 4 have again been identified in overlapping regions ('tongues') of parameter space, arising in distinct frequency bands, associated with which are transverse wavelike displacements of the internal core flow downstream of the oscillating membrane; these are low frequency, long wavelength Tollmien–Schlichting (TS) waves, often referred to in this context as vorticity waves. While distinct oscillatory modes were captured also in 1D [14], it is clearly not possible to describe TS waves in a 1D framework and their role in the underlying instability mechanism remains to be fully understood.

Improvements in computational power in the last decade, plus the development of algorithms in which fluid and solid mechanics problems are solved in a fully coupled (monolithic) manner [19], have recently allowed 3D simulations of the Starling Resistor to become feasible. Finite-element simulations coupling geometrically nonlinear shell theory to a steady Navier–Stokes solver were reported by Hazel & Heil [20]; there has also been success in simulating steady flow solutions using a commercial package [21]. Something of a milestone in the history of this problem was passed at the XXII ICTAM with the first report of fully unsteady 3D simulations of self-excited oscillations in the Starling Resistor [22], which involve transitions between distinct buckled states (illustrated schematically in Fig. 5(b) below).

A parallel strand of research has addressed instabilities of flows in homogeneous flexible channels. Here, wave-like solutions of the linearized Navier–Stokes equations are sought, satisfying boundary conditions capturing properties of a deformable wall (bending stiffness, tension, springs, damping, inertia, etc.). Multiple modes of local instability have been identified, and it is useful to consider how they may be related to the global instabilities arising in the Starling Resistor. Briefly, the local modes are classified into four major groups [23, 24, 25]: static divergence (SD); TS waves; travelling-wave flutter (TWF); and interactive modes. A global SD instability is responsible for the multiple static modes seen in 1D [13] and 2D [16] analyses of finite-length collapsible tube or channel flows: SD can arise through both viscous and inertial mechanisms. TS waves (evident in 2D simulations [17]) arise of course in rigid-walled channels but in the presence of a flexible wall they can be destabilized by wall damping. In contrast, TWF is stabilized by wall damping (requiring energy to be transferred from the flow to the wall).

Connections between local and global modes of instability in the context of a 1D model are now explored further, and energy methods are used to distinguish between distinct mechanisms of global instability in the Starling Resistor.

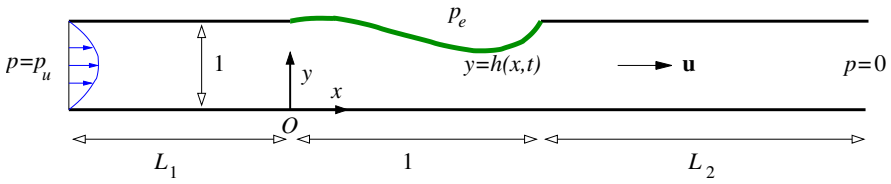

Fig. 2. The 2D analogue of the Starling Resistor. Flow is driven by a fixed pressure drop p_u through a finite-length channel, one wall of which contains a flexible membrane under external pressure $p_e(x)$. Distances x and y along and across the channel are scaled on the length of the flexible segment and the channel width.

3 A one-dimensional model

A recent study [26] of a 1D model of flow in a 2D collapsible channel (Fig. 2) has revealed a number of significant features of self-excited oscillations, which we review briefly here. Consider the flow driven by a prescribed pressure drop through the 2D analogue of the Starling Resistor (Fig. 2). An external pressure distribution is prescribed that exactly matches the linear pressure drop that would arise if the channel were uniform. This enables the system to support the uniform flow state as a steady solution. The membrane is held under longitudinal tension. The 2D Navier–Stokes equations describing the flow through the channel are reduced to the boundary-layer equations by making a long-wavelength approximation. A further reduction to a 1D system is achieved by making a von Kármán–Pohlhausen aproximation, whereby a prescribed parabolic velocity profile is assumed, enabling the mass and momentum equations to be integrated across the channel. The resulting model equations expressing mass and momentum conservation are, in dimensionless form [26],

$$h_t + q_x = 0, \tag{1a}$$

$$q_t + \frac{6}{5}\left(\frac{q^2}{h}\right)_x = Thh_{xxx} + \frac{12}{R}\left(h - \frac{q}{h^2}\right) \tag{1b}$$

along the length of the flexible segement of channel in $0 < x < 1$. Here $h(x,t)$ is the channel width and $q(x,t)$ the axial volume flux. The rigid segment of channel upstream has relative length L_1 and that downstream L_2. Attention is focused on the case $L_1 < L_2$, for reasons explained below. Additional dimensionless parameters are a Reynolds number R and a membrane tension parameter T; the term $12h/R$ arises from the choice of external pressure distribution. The model is expected to be reliable for $R \lesssim 1$, when viscous effects are dominant, but potentially unreliable for $R \gg 1$ or for high frequency motion. Equations (1a,b) are solved subject to boundary conditions

$$h = 1, \qquad Th_{xx} = L_1\left[\frac{12}{R}(q-1) + q_t\right] \qquad (x = 0), \tag{1c}$$

$$h = 1, \qquad Th_{xx} = -L_2\left[\frac{12}{R}(q-1) + q_t\right] \qquad (x = 1), \tag{1d}$$

which account for the pressure drop associated with viscous dissipation and unsteady inertia in the upstream and downstream rigid channel segments. Eqs (1a-d) admit the uniform steady solution $h = 1$, $q = 1$, enabling straightforward linear stability analysis of this state.

It is useful first to consider the dispersion relation for small-amplitude wavelike disturbances of wavenumber k and frequency ω arising in the flexible segment of the channel, satisfying the linearised form of Eqs (1a,b). This is

$$\omega^2 + \frac{6}{5}\left(k^2 - 2\omega k\right) - Tk^4 - \frac{12i}{R}(3k - \omega) = 0. \tag{2}$$

Analysis of Eq. (2) in the complex k and ω planes using the Briggs–Bers condition reveals that any unstable disturbances are convectively, but not absolutely unstable, with the large-time response to point forcing arising through an interaction of an evanescent upstream SD mode and an unstable downstream TWF mode [26]. Thus any instabilities that arise in the finite-length system cannot involve absolute instability of these modes.

In order to account for boundary conditions, a global linear stability analysis is necessary. Looking for small disturbances to the uniform state with time dependence $e^{\sigma t}$, a fourth-order eigenvalue problem must be solved. This reveals multiple modes of static and dynamic instability. Neutral curves in the (R, T)-plane are identified across which static modes arise through transcritical bifurcations (where $\sigma = 0$) and oscillatory modes arise through Hopf bifurcations (where $\mathrm{Re}(\sigma) = 0$). Following the convention mentioned previously, modes are labelled by the number of extrema in h. The uniform state is linearly stable for high tension and low Reynolds number. If T is reduced for fixed low R, the uniform state bcomes unstable to static mode 1 and mode 2 instabilities, through a global viscous SD instability. Alternatively, if R is increased for fixed $T \gg 1$, the uniform state becomes unstable to an oscillatory mode 1 instability, which has high frequency because of the large membrane tension.

Although this 1D model is not expected to be quantitatively reliable for high-frequency motion, the oscillatory mode 1 instability arising for $T \gg 1$ turns out to be worthy of analysis. An asymptotic approximation can be constucted by expanding variables in powers of $T^{-1/2}$. At leading order, the flux perturbation $Q_0(x)$ satisfies a fourth-order self-adjoint eigenvalue problem parameterized only by L_1 and L_2, involving a balance between unsteady inertia and membrane tension. This reveals a normal mode of the system, in which transverse oscillations of the wall drive an axial oscillatory sloshing motion of the fluid within the entire channel. This is independent of the imposed mean flow to this order. Because $L_1 < L_2$, the amplitude of sloshing is larger in

the upstream rigid segment than downstream (i.e. $|Q_0(0)| > |Q_0(1)|$). At the following order in $T^{-1/2}$, the mean flow, convective inertia and viscous effects enter the problem. A solvability condition enables a critical Reynolds number to be identified

$$R_1 = \frac{10\left[L_1 Q_0^2(0) + L_2 Q_0^2(1) + \int_0^1 Q_0^2 \,\mathrm{d}x\right]}{Q_0^2(0) - Q_0^2(1)}. \tag{3}$$

This can be interpreted as a ratio of viscous dissipation to kinetic energy flux. Critically, the asymmetry of the system ($L_1 < L_2$) induces asymmetry in the eigenmode; more vigorous sloshing at the upstream end of the channel allows the instability to extract more energy from the mean flow entering the flexible segment of channel than is swept out of its downstream end. The system can therefore be destabilized by increasing the ratio L_2/L_1, which might be achieved by prescribing the downstream flux (setting $L_2 \to \infty$) or minimising upstream inertance. In systems for which the upstream flux is prescribed ($L_1 \to \infty$), instability of the uniform state is not expected to arise through this mechanism. The asymptotic estimate Eq. (3) for $T \gg 1$ agrees well with predictions of the full stability calcluation [26].

Further analysis [26] shows that the mode 1 instability contains four independent components (two TWF modes and two SD modes, with one of each type propagating upstream and downstream), and that global instability can arise when all four component modes are convectively stable. Analysis of the history of a disturbance as it propagates upstream, reflects from the rigid segment at $x = 0$, propagates downstream and reflects from $x = 1$ (following [27]) confirms that growth arises from reflections at the boundaries of the flexible segment of channel.

A further notable feature of the mode-1 instability is that, as its amplitude grows, the unsteady sloshing induces a steady pressure gradient along the flexible segment of channel through the action of Reynolds stresses (via the nonlinear q^2/h term in Eq. (1b)). As the pressure drop across the channel is assumed fixed, the effect is to induce an adjustment to the mean flux of the form [26]

$$\overline{q} = 1 + \frac{7RA^2}{240(1 + L_1 + L_2)}\left[Q_0^2(0) - Q_0^2(1)\right], \tag{4}$$

where A is the amplitude of the oscillation. Thus the mode 1 oscillation acts as a pump, increasing the mean flux. As a consequence, mode 1 can arise through a subcritical Hopf bifurcation.

Finally, it is instructive to examine the energy budget of the mode 1 instability. Integrating the energy transport equation over the domain, and averaging over a period of a neutrally stable oscillation, yields an equation of the form

$$\overline{\mathcal{F}} + \overline{\mathcal{P}} = \overline{\mathcal{D}} \tag{5}$$

where $\overline{\mathcal{F}}$ is the net kinetic energy flux, $\overline{\mathcal{P}} = \frac{6}{5} p_u \overline{q}$ is the net work-rate by the upstream pressure, and $\overline{\mathcal{D}}$ is the net viscous dissipation rate. The choice of wall

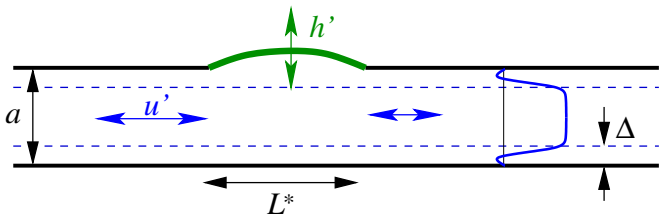

Fig. 3. Sloshing in a 2D channel: the membrane length L^* exceeds the channel width a; transverse wall motions of amplitude h' drive axial flows of magnitude u'; at high frequencies, Stokes layers of width Δ are thin compared to the channel width.

model implies that zero net work is done on the flexible wall over an oscillation. The denominator in Eq. (3) is proportional to $\overline{\mathcal{F}}$, which must be positive in order to sustain the mode 1 instability. Significantly, numerical simulations of Eqs (1) for an oscillatory mode 2 instability (a secondary instability of a static mode 2 state, arising at lower T) exhibit $\overline{\mathcal{F}} < 0$, indicating that work done by the upstream pressure $\overline{\mathcal{P}}$ provides the source of energy in this case. This mechanism is a likely candidate for the instabilities observed in 2D simulations with prescribed upstream flux [17, 18].

In summary, the 1D model shows that high-frequency mode 1 oscillations arise through wave reflections, not local instability. Asymmetric boundary conditions ($L_1 < L_2$) allow energy to be extracted from the mean flow via kinetic energy fluxes. However, this mechanism is not universal, and other modes may, for example, rely on work done by the upstream pressure as the source of energy.

4 A two-dimensional model

The 1D approach is attractive as analysis is relatively straightforward. However the model described above is predicated on an assumption about the velocity profile that is not uniformly valid across parameter space. In particular, at high frequencies, oscillatory viscous boundary layers (Stokes layers) can be expected to form on the walls of the channel, which were not resolved within the 1D approach. It is therefore desirable to revisit the 2D problem illustrated in Fig. 2 within a fully 2D framework, avoiding any *ad hoc* assumptions. This approach was adopted by Jensen & Heil [28], in a study combining high Reynolds number asymptotics and full simulation of the 2D system, assuming uniform external pressure.

The mode 1 oscillatory instability in a 2D channel is described asymptotically by assuming disturbances are of long wavelength compared to the channel width, and of sufficiently high frequency for viscous effects to be confined to Stokes layers. The leading-order inviscid 'sloshing' behaviour identified in the 1D model carries over directly to 2D. It is helpful to revisit the scaling

argument that captures the primary physical balances, using the dimensional variables illustrated in Fig. 3. Neutrally stable unsteady sloshing at frequency ω involves a balance between unsteady inertia and an axial pressure gradient (i.e. $\rho u_t \sim p_x$, where '$\sim$' denotes 'scales like' and ρ is density) giving a balance $\rho\omega u' \sim p'/L^*$; the pressure is proportional to the curvature of the membrane ($p \sim T^* h_{xx}$) but the high tension ensures deflections are small ($p' \sim T^* h'/L^{*2}$); because the channel is slender, axial flows are larger than transverse ones ($u_x \sim v_y$ implies $v' \sim au'/L^*$); transverse fluid velocities balance wall motion ($v \sim h_t$ implies $v' \sim \omega h'$). Combining these relations yields the frequency estimate $\omega^2 \sim T^* a/\rho L^{*4}$. An energy balance (following Eq. 5) determines the conditions necessary for neutral stability. Viscous dissipation takes place in Stokes layers, of thickness $\Delta \sim (\mu/\rho\omega)^{1/2} \ll a$. For $L_2 > L_1$, the rate of dissipation must balance the net kinetic energy flux into the flexible segment ($\rho U_0 u'^2 a \sim \mu\overline{(u'^2/\Delta^2)}\Delta L^*$), which yields a critical Reynolds number

$$Re = \frac{\rho U_0 a}{\mu} \sim \left(\frac{\rho T^* a}{\mu^2}\right)^{1/4}. \tag{6}$$

This scaling differs from the predictions of the 1D model, because the 1D model used an inconsistent description of viscous dissipation. Detailed analysis is required to determine the coefficient in Eq. (6), which must also be validated against direct numerical simulation [28].

The analysis is pursued in a distinguished limit involving a single small parameter $\delta \ll 1$, whereby the channel length scales like $\delta^{-1/2}$, Reynolds number like $\delta^{-3/2}$ and membrane tension like δ^{-3}. The Navier–Stokes and membrane equations (with uniform p_e) then reduce with error $O(\delta^3)$ to

$$\begin{aligned}
u_x + v_y &= 0 \\
u_t + \delta(\mathbf{u}\cdot\nabla)u &= -p_x + \delta^2 r^{-2} u_{yy} \\
\lambda\delta[v_t + \delta(\mathbf{u}\cdot\nabla)v] &= -p_y \\
u = 0,\ v = h_t,\ p &= p_e - h_{xx} && (y = 1 + \delta h) \\
u = v &= 0 && (y = 0) \\
p &= 12\delta^2 r^{-2}(1 + L_1 + L_2) && (x = -L_1) \\
p &= 0 && (x = 1 + L_2)
\end{aligned}$$

with λ, r, L_1 and L_2 treated as $O(1)$ parameters as $\delta \to 0$. An expansion is constructed, setting $\mathbf{u} = \mathbf{u}_0 + \delta\mathbf{u}_1 + \delta^2\mathbf{u}_2 + \ldots$, with

$$\begin{aligned}
u_0 &= u_{00} + u_{01}e^{i\beta t} + \bar{u}_{01}e^{-i\beta t} \\
u_1 &= u_{10} + u_{11}e^{i\beta t} + \bar{u}_{11}e^{-i\beta t} + u_{12}e^{2i\beta t} + \bar{u}_{12}e^{-2i\beta t} \\
u_2 &= u_{20} + \ldots
\end{aligned}$$

for some $O(1)$ frequency β to be determined, with bars denoting complex conjugates and coefficients depending on slow timescales $t_1 = \delta t$, $t_2 = \delta^2 t$, etc.

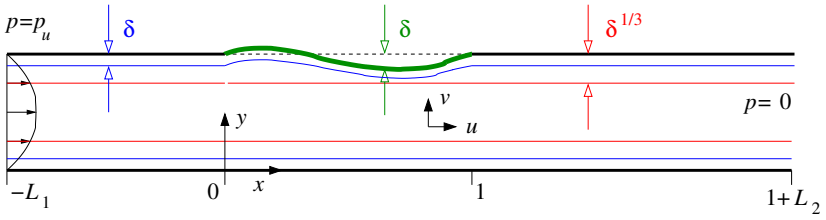

Fig. 4. The asymptotic structure of sloshing flows in a 2D channel. Stokes layers have dimensionless thickness $\delta \ll 1$; membrane displacements are $O(\delta)$; steady streaming boundary layers have thickness $\delta^{1/3}$.

The physical structure of the asymptotic problem is illustrated in Fig. 4. In problem 00, the membrane is deflected slightly by the mean pressure ($h_{00} = -\frac{1}{2}p_e x(1-x)$) and the mean flux is uniform Poiseuille flow ($u_{00} = 6q_{00}y(1-y)$, $v_{00} = 0$, $p_{00} = 0$), but with the flux q_{00} undetermined to this order. Stokes layers of thickness $O(\delta)$ appear in problems 01, 11; a Prandtl transformation is used to wrap the upper Stokes layer onto the membrane (Fig. 4). Steady-streaming boundary layers of thickness $O(\delta^{1/3})$ appear in problems 10 and 20. The inviscid sloshing mode appears in problem 01. The leading-order eigenmode $h_{01} = A(t_1)\phi_{01}(x)$, where A is a slowly varying amplitude, is determined exactly as in the 1D model (Sec. 3). Interaction between the mean flow and the sloshing motion arises in problem 11, where again a solvability condition is imposed to determine a condition for neutral stability in terms of the rescaled Reynolds number

$$r = \frac{(2\beta)^{\frac{1}{2}}}{q_{00}} \frac{\int_0^1 \phi_{01x}^2 \, \mathrm{d}x}{\phi_{01x}^2(1) - \phi_{01x}^2(0)}, \tag{7}$$

which is positive for $L_2 > L_1$. This expression provides the coefficient in (6). However the mean flux q_{00} remains undetermined to this order. To determine q_{00}, it is necessary to consider the time-averaged Reynolds stresses $\overline{(\mathbf{u}_0 \cdot \nabla)u_0}$, which create a steady pressure gradient in the core to which q_{00} must adjust (the analogue of Eq. (4)). Further contributions to the mean flow come from steady streaming driven by Stokes layers and by deflection due to indentation of the membrane by p_e.

The energy budget for the neutral oscillation is again given by Eq. (5), where the dissipation rate can be partitioned into a contribution from the Stokes layers $\overline{\mathcal{D}_S}$ plus that in the core $\overline{\mathcal{D}_P}$. Accounting for mean flow adjustment, this partition turns out to be in a precise 2:1 ratio, with $\overline{\mathcal{D}_S} = \frac{2}{3}\overline{\mathcal{F}} > 0$, $\overline{\mathcal{D}_P} = \overline{\mathcal{P}} + \frac{1}{3}\overline{\mathcal{F}}$.

The asymptotic prediction Eq. (7) with $q_{00} = 1$ was tested against simulations conducted using a finite-element method in which the Navier–Stokes and membrane equations were fully coupled [28]. The initial-value problem was solved following a jump in p_e. For $\delta = 0.3$ — not a particularly small value — the predicted transitional Reynolds number (around 400) differed

from that determined by simulation by less than 10%; predicted frequencies and growth rates were more accurately predicted for smaller δ. Thus the mechanism of mode 1 oscillation identified (albeit qualitatively) in the 1D model therefore carries through to 2D, where it can be described using rational validated asymptotics.

5 Towards a three-dimensional model

Having identified a mechanism of instability in a flexible channel using an approximate 1D approach (Sec. 3), and produced a refined asymptotic description of its operation in 2D (Sec. 4), the next obvious step is to ask how this mechanism might operate in a more realistic 3D tube.

Heil & Waters [29] addressed this problem theoretically by considering axial sloshing flows generated in a circular tube. They prescribed periodic wall motions with azimuthal mode number 2 (resembling elliptical post-buckled configurations) of small ($O(\epsilon)$) amplitude, high frequency and long wavelength. Because the base state they examined was axisymmetric, the area change during an oscillation was small and the induced sloshing was of magnitude $O(\epsilon^2)$, with transverse oscillations being decoupled from the axial flow. While such weak sloshing inhibits energy transfer from the mean flow via kinetic energy fluxes, the decoupling made it feasible to study the transverse flow-structure interaction, with wall bending balancing unsteady fluid inertia, and viscous dissipation (in Stokes layers and the core) determining the decay rate of oscillatory modes. The imposed symmetry of the computations accommodated buckled states symmetric about orthogonal axes, with the primary buckling being either horizontal or vertical (cross-sections are illustrated schematically in Fig. 5(a)). Large-amplitude oscillations decayed first by switching between these two states during each period (motion denoted as 'Type I' in [29]), before jumping to one of the two states (becoming a 'Type II' oscillation) and then decaying towards the corresponding equilibrium buckled configuration. The dynamics is reminiscent of a Duffing oscillator, and is illustrated in a schematic phase plane in Fig. 5(a). The switch from Type I to Type II can then be interpreted as the passage of a trajectory in phase space past a saddle point corresponding to the unbuckled equilibrium state. It is notable that recently reported 3D simulations of self-excited oscillations [19, 22] exhibit sustained Type-I oscillations, illustrated schematically by the limit cycle in Fig. 5(b). This in turns suggests the likelihood of homoclinic bifurcations arising from the collision of limit cycles with fixed points, reported in this context in [9].

To ensure that transverse wall motion would generate a strong axial sloshing flow, Heil & Waters [30] then computed the unsteady 3D flow through a non-axisymmetric tube, a segment of which underwent prescribed small-amplitude wall motion of frequency ω. This motion was formulated as a set of Fourier modes in axial and azimuthal coordinates for which the tube perime-

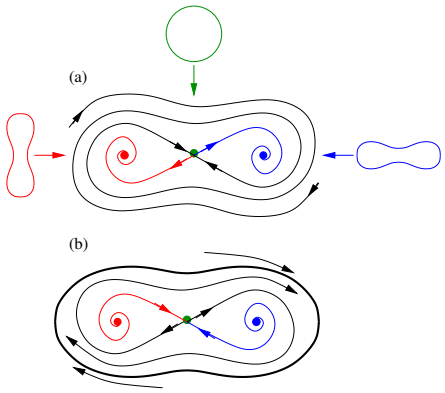

Fig. 5. (a) A phase portrait of a Duffing oscillator, which captures the dominant dynamics of decaying oscillations in an elastic ring, reported in [29]. Initial large-amplitude Type-I oscillations that flip between vertically and horizontally buckled states ultimately decay to smaller-amplitude Type-II oscillations in one of the two states. Cross-sections at fixed points are illustrated. (b) A stabe limit cycle of Type I.

ter was preserved. The non-axisymmetric base state, combined with area-changing perturbations of $O(\epsilon)$ amplitude, ensured $O(\epsilon)$ sloshing. The flux at the downstream end of the tube was prescribed, a condition expected to promote kinetic energy transfer from the mean flow (as explained following Eq. 3). Simulations showed how energy could indeed be transferred to the wall, provided α/St exceeded a threshold (where $\alpha = a(\rho\omega/\mu)^{1/2}$ is the Womersley number, $St = a\omega/\mathcal{U}$ the Strouhal number, a an effective tube radius and $\mathcal{U}$ a measure of the imposed axial flow), again reflecting a balance of kinetic energy flux with dissipation in Stokes layers.

This finding has been generalised in a recent study by Whittaker et al. [31] in which the necessary asymptotic conditions for prescribed wall motion to extract energy from the mean flow have been identified. Here flow through a tube is considered in which the shape of the cross-section is arbitrary except that it varies slowly in the axial direction and exhibits small-amplitude temporal oscillations. The tube centreline is straight and lies on $0 < z < L$. Oscillations about the base state are prescribed, and a flow is driven through the tube under fixed flux or under prescribed pressure drop. The tube kinematics can be characterized using just a handful of quantities: the perimeter $\mathbb{P}(\check{z})$ and cross-sectional area $A_0(\check{z})$ of the base state (as a function of axial distance $\check{z} = z/L$); the oscillatory area change in each cross-section $\mathbb{A}(\check{z})$; and the volume variation along the tube $\mathbb{V}(\check{z})$ arising from the axially integrated area changes. The flow is characterized by Strouhal and Womersley numbers (St and α, as defined above), tube length $\ell = L/a$ and oscillation amplitude Λ. Once again, a distinguished limit is considered in which the kinetic energy

flux balances dissipation in Stokes layers, and wall motions are assumed to be long wave and small amplitude, i.e.

$$1 \ll \alpha \sim \ell St \sim \ell^2 \ll \frac{1}{\Lambda}. \tag{8}$$

The asymptotic approach to this problem follows that outlined in Secs 3 and 4, but inevitably is more involved. Variables are decomposed into steady, period-1 and period 2 or greater, in the core and in Stokes layers, and the Navier–Stokes equations are decomposed accordingly. The system is expanded in powers of the small amplitude, with the core and boundary-layer problems being treated separately. The leading-order inviscid sloshing problem is governed by a Poisson problem; associated Stokes layers eject flux into the core. Sloshing generates Reynolds stresses, the steady component of which adjusts the dimensionless mean flux $\mathbb{Q}$ (under prescribed pressure conditions) or the net pressure drop (when the flux is prescribed). The energy budget for small amplitude periodic oscillations, integrated over the flow domain, is expressed as

$$\mathcal{E} = \mathcal{F} + \mathcal{P} - \mathcal{D}, \tag{9}$$

where $\mathcal{E}$ is the work done on the wall by the fluid, $\mathcal{F}$ is the kinetic energy flux, $\mathcal{P}$ is the work done by the upstream pressure and $\mathcal{D}$ the dissipation. Decomposition of Eq. (9) into steady and oscillatory components allows the former to be studied independently. As for the 2D problem (Sec. 4), there is a remarkably precise partition of energy, with 2/3 of the kinetic energy flux due to sloshing being available to do work on the walls and the remaining 1/3 being dissipated in the mean flow or doing work against pressure at the tube ends. The condition that there is zero energy transfer to the wall over a period (Eq. (5)) yields a simple condition on the inverse Strouhal number (or equivalently a critical Reynolds number α^2/St_c) that resembles Eqs (3) and (7) in being the ratio of viscous dissipation to kinetic energy flux, this ratio being expressed in the form [31]

$$\frac{\alpha}{\ell St_c} \sim C(\mathbb{Q}; \mathbb{V}, A_0, \mathbb{P}) \tag{10}$$

where C is a functional of the kinematic variables. Eq. (10) has been validated against 3D simulations in an elliptical tube with prescribed wall motion [31], showing good agreement across a range of α and ℓ for both prescribed flux and prescribed pressure boundary conditions. Further work is required to test this stability prediction when the prescribed wall displacement is replaced by a normal mode of the tube, accounting for fully unsteady 3D flow-structure interaction.

6 Discussion

This brief review has hopefully demonstrated the usefulness of using a hierarchy of models to understand instabilities of flows in the Starling Resistor. In

particular, low-dimensional approximations have provided valuable signposts for more elaborate asymptotic and computational models. Stability thresholds of increasing accuracy ((3), (7) and (10)) have been used to characterise a potential mechanism of high-frequency self-excited oscillation. Further steps are needed to establish a definitive connection between this mechanism and what happens in the real experimental device: in particular, unsteady simulations of the 3D problem must be analysed to establish the nature of energy budgets, and the simulations must themselves be validated against experiment. It is important to recognise also that the 'sloshing' mechanism described above is not generic: the 1D model shows how oscillations with a quite distinct energy signature can arise [26] where the dominant energy source is work done by the upstream pressure, from which oscillations may be able to sustain themselves by increasing the mean flux. Simulations in 2D highlight a potential role for internal hydrodynamic modes [17, 18], and recent 3D simulations demonstrate the dominant role of buckling instabilities [20, 22].

The distinguished physiologist Ernest Starling [4] will not have appreciated how much he contributed to the study of flow-structure interaction by inventing his Resistor.

Acknowledgements

Jonathan Boyle, Matthias Heil, Peter Stewart, Sarah Waters and Robert Whittaker have contributed to many of the developments reported above. Support from the Royal Society is gratefully acknowledged. This article is dedicated to the memory of Peter W. Carpenter (1942–2008), who made lasting and profound contibutions to the study of flows interacting with compliant surfaces.

References

1. Pedley TJ, Brook BS, Seymour RS (1996) Blood pressure and flow rate in the giraffe jugular vein. Phil Trans Roy Soc B 351: 855–866
2. Heil M, Jensen OE (2003) Flows in deformable tubes and channels - Theoretical models and biological applications. In: Carpenter PW, Pedley TJ (eds) Flow past highly compliant boundaries and in collapsible tubes, IUTAM Proceedings Vol. 72, Springer
3. Grotberg JB, Jensen OE (2004) Biofluidmechanics of flexible tubes. Ann. Rev. Fluid Mech. 36:121–147
4. Knowlton FP, Starling EH (1912) The influence of variations in temperature and blood-pressure on the performance of the isolated mammalian heart. J Physiol London 44:206–219
5. Bertram CD, Raymond CJ, Pedley TJ (1990) Mapping of instabilities for flow through collapsed tubes of differing length. J Fluids Struct 4:125–153

6. Bertram CD, Tscherry J (2006) The onset of flow-rate limitation and flow-induced oscillations in collapsible tubes. J Fluids Struct 22:1029–1045
7. Pedley TJ, Luo XY (1998) Modelling flow and oscillations in collapsible tubes. Theor Comput Fluid Dyn 10:277–294
8. Bertram CD, Pedley TJ (1982) A mathematical model of collapsible tube behaviour. J Biomech 15:39–50
9. Armitstead J, Bertram CD, Jensen OE (1996) A study of the bifurcation behaviour of a model of flow through a collapsible tube. Bull Math Biol 58: 611–641
10. Shapiro AH (1977) Steady flow in collapsible tubes. J Biomech Engng 99: 126–147.
11. Cancelli C, Pedley TJ (1985) A separated-flow model for collapsible-tube oscillations. J Fluid Mech 157: 375–404
12. Hayashi S, Hayase T, Kawamura H (1998) Numerical analysis for stability and self-excited oscillation in collapsible tube flow. J Biomech Engng 120: 468–475
13. Jensen OE, Pedley TJ (1989) The existence of steady flow in a collapsed tube. J Fluid Mech 206: 339–374
14. Jensen OE (1990) Instabilities of flow in a collapsed tube. J Fluid Mech 220: 623–659
15. Pedley TJ (1992) Longitudinal tension variation in collapsible channels: a new mechanism for the breakdown of steady flow. J Biomech Engng 114:60–67
16. Guneratne J, Pedley TJ (2006) High Reynolds number steady flow in a collapsible channel. J Fluid Mech 569: 151–184
17. Luo XY, Pedley TJ (1996) A numerical simulation of unsteady flow in a two-dimensional collapsible channel. J Fluid Mech 314:191–225
18. Luo XY, Cai ZX, Li WG, Pedley TJ (2008) The cascade structure of linear instability in collapsible channel flows. J Fluid Mech 600:45–76
19. Heil M, Hazel AL, Boyle J (2008) Solvers for large-displacement fluid-structure interaction problems: segregated versus monolithic approaches. Comput Mech 43:91–101
20. Hazel AL, Heil M (2003) Steady finite Reynolds number flows in three-dimensional collapsible tubes. J Fluid Mech 486:79–103
21. Marzo A, Luo XY, Bertram CD (2005) Three-dimensional collapse and steady flow in thick-walled flexible tubes. J Fluids Struct 20:817–835.
22. Heil M, Boyle J (2008) Recent progress in the theoretical and computational modelling of flow in 3D collapsible tubes, XXII ICTAM, Adelaide, Australia
23. Benjamin TB (1963) The threefold classificion of unstable disturbances in flexible surface bounding inviscid flows. J Fluid Mec 16:436–450
24. Landahl M (1962) On the stability of a laminar incompressible boundary layer over a flexible surface. J Fluid Mech 13: 609–632
25. Davies C, Carpenter PW (1997) Instabilities in plane channel flow between compliant walls. J Fluid Mech 352:205–243
26. Stewart PS, Waters SL, Jensen OE (2008) Local and global instabilities of flow in a flexible-walled channel (submitted)
27. Doaré O, de Langre E (2006) The role of boundary conditions in the instability of one-dimensional systems. Eur J Mech B 25:948–959
28. Jensen OE, Heil M (2003) High-frequency self-excited oscillations in a collapsible-channel flow. J Fluid Mech 481: 235–268
29. Heil M, Waters SL (2006) Transverse flows in rapidly oscillating elastic cylindrical shells. J Fluid Mech 547: 185–214

30. Heil M, Waters SL (2008) How rapidly oscillating collapsible tubes extract energy from a viscous mean flow. J Fluid Mech 601: 199–227
31. Whittaker RJ, Waters SL, Jensen OE, Boyle J, Heil, M. (2008) The energetics of flow through a rapidly oscillating tube. Part I: general theory. Part II: application to an elliptical tube. (preprint)